

## MODELING THE LICK/IDS SPECTRAL FEATURE INDICES USING SYNTHETIC SPECTRA

MICHAEL J. TRIPICCO<sup>1</sup> AND R. A. BELL

Department of Astronomy, University of Maryland, College Park, Maryland 20742-2421

Electronic mail: miket@astro.umd.edu, rabell@astro.umd.edu

Received 1995 July 5; revised 1995 August 31

## ABSTRACT

A group at Lick Observatory has measured spectral indices for stars, globular clusters, and galaxies. As part of a program to compute integrated spectra and colors for clusters and galaxies, we have modeled these indices for stars. This comparison is intended in part as a test of the synthetic indices and their value in modeling the other objects and in part as an attempt to obtain new insights, such as the dependence of the indices on the abundances of individual elements. Since we have shown previously that a 5 Gyr isochrone matches the color–magnitude diagram of M67 very well [AJ, 106, 618 (1993)], we have calculated synthetic spectral indices for temperature and gravity points along this isochrone. Our values, plotted as index versus temperature diagrams, have been compared with observations of M67 stars and field stars, the latter mostly being objects whose atmospheric parameters are similar to the isochrone values. These comparisons show generally good agreement and indicate that model cluster and galaxy spectra should yield valuable insights when compared to the corresponding observations. We studied the changes of the indices produced by changes in bandpasses and smoothing, results which may be of value to other observers, and to changes in overall metal abundance and in changes of the abundances of individual elements. While these latter changes give specific values for results which would be anticipated, such as the dependence of the Na D index on sodium abundance, they also show that many other indices vary only weakly with abundance or vary a great deal in an unexpected way. For example, the Fe4668 index is very sensitive to changes in carbon abundance. In addition, it is difficult to find the Fe abundance using the Lick indices, only one index being more sensitive to changes in Fe itself than to changes in the overall metal abundance. © 1995 American Astronomical Society.

## 1. INTRODUCTION

Over the past two decades, Faber and colleagues at Lick Observatory have compiled an extensive and homogeneous spectral database for stars, globular clusters, and galaxies. The information contained within these spectra has been quantified by using a system of 21 spectral indices which measure the strength of strong atomic and molecular absorption-line features (Worthey *et al.* 1994, hereafter referred to as WFGB94). These indices have been distilled into empirical polynomial fitting functions which give index strengths as a function of fundamental stellar parameters, with an aim toward using these to construct stellar population models (e.g., Buzzoni 1995).

However, this approach is limited in several important ways because the calibration is based on Galactic stars. For example, the metallicity range of the original fitting functions is limited to [Fe/H] between  $-1$  and  $+0.5$  dex (WFGB94) although they have recently been extended to lower metallicities by Idiart & Freitas Pacheco (1995). More importantly, empirical methods do not allow for nonstandard abundance ratios in constructing integrated light models despite strong evidence, for example, that magnesium is significantly enhanced relative to iron in giant elliptical galaxies (Worthey *et al.* 1992) and that cyanogen band strengths in

M31 globular cluster spectra are extremely high (see review by Tripicco 1993, and references within).

By using synthetic stellar spectra we can avoid these problems and thus our ultimate goal is to produce wholly theoretical integrated light spectra which can be compared with spectra of galaxies and other composite stellar populations. But the individual stellar spectrum models can themselves be used to more carefully determine the sensitivities of the absorption features (as seen at moderate resolution) to changes in temperature, gravity, and especially to variations in individual element abundances. As we will show in this paper, spectral indices sometimes behave in unexpected ways.

The Lick stellar data and associated fitting functions also provide an excellent basis by which to evaluate the quality of the synthetic spectra themselves over a broad range in stellar effective temperature and surface gravity. Another important aspect of this paper, therefore, is to use the comparison between observed and predicted spectral indices to point out trouble spots in the synthetic spectra and to guide us in the process of fine tuning the critical input atomic and molecular data (i.e., oscillator strengths and/or radiative damping constants). In this way we can decide *a priori* which spectral indices will be most or least reliable in the context of our integrated light models. Finally, we have investigated the dependence of the indices to various quantities, including the abundances of individual elements.

This paper represents the most comprehensive effort to date in simulating the full set of Lick/IDS spectral indices

<sup>1</sup>Present address: Mail Code 664, NASA/Goddard Space Flight Center, Greenbelt, MD 20771.

and in including element ratio variations. Previous work has tended to focus almost entirely on the magnesium features around 5175 Å (e.g., Chavez, *et al.* 1995, and earlier papers by the same group) and has generally not included non-standard abundance ratios. While McQuitty *et al.* (1994) were able to vary [Mg/Fe] and other element ratios, they too restricted themselves to the Mg and Fe features between 4900 and 5500 Å and their indices were not designed to simulate the Lick/IDS system (although they are quite similar).

The remainder of the paper is organized in the following fashion. Section 2 describes the calculation of the synthetic spectra, their distribution in  $T_{\text{eff}}$  and  $\log g$ , and the procedures we use in measuring the spectral indices. Examples of high-dispersion spectra for the Sun and for Arcturus compared with our models for these benchmark stars are also shown to indicate the quality of the fits of our spectra to the corresponding stars. Section 3 presents the detailed index-by-index comparisons between theory and observation (on a star-by-star basis as well as via the empirically defined polynomial fitting functions), plus tabulations of the sensitivity of each index to various physical and computational parameters. A discussion of the results is given in Sec. 4 (including notes on individual indices) and Sec. 5 presents some concluding remarks.

## 2. MODEL CALCULATIONS

### 2.1 Synthetic Spectra

The model results discussed in this paper are based on a 5 Gyr solar abundance isochrone which we have previously shown (Tripicco *et al.* 1993, hereafter referred to as TDB93) to provide a good fit to the color–magnitude diagram for the open cluster M67. The construction of the isochrone is detailed in that paper. We have, however, recomputed all of the model atmospheres and synthetic spectra at 56 closely spaced intervals along the isochrone so as to include a number of improvements which have since been made to our line list and to the atomic and molecular data.

The values of several of the Lick indices depend upon the strengths of strong lines, e.g.,  $\lambda 4227$  of Ca I, the Mg *b* lines and the Na D lines. The broadening of these lines in the Sun and other cool dwarfs is dominated by the collisional damping. The pressure dependence of this broadening can be used to deduce the gravities of stars from the profiles of strong lines (Blackwell & Willis 1977). However, the lower pressures in the atmospheres of giants lead to radiative damping becoming a much more significant contributor to the total damping. In fact, Edvardsson (1988) points out that the lines of the Ca infrared triplet show an inverse dependence on gravity, since they have very large radiative damping constants owing to sharing levels with the H and K lines. Consequently, we calculated radiative damping constants for many additional strong lines of a number of elements, e.g., Na–Si, Sc–Cu. The new, electronically readable, multiplet table for Fe I (Nave *et al.*, 1994) made finding these data more convenient for this species than for other elements, where the Revised Multiplet Tables (Moore 1945) had to be used to find lines arising from the same levels. This change

in the damping yielded a perceptibly better fit to the profiles of some of the strong lines (e.g., the Mg *b* lines) in the spectrum of Arcturus.

In view of the importance of the G band in this study, the wavelengths of the *A–X* CH lines have been reexamined. Some of these were originally obtained from Gerö (1941). A number of wavelength changes were made earlier, using the work of Krupp (1973). Additional improvements were made for this paper using the newer data of Bembenek *et al.* (1990) and Bernath *et al.* (1991). However, it is still necessary to use calculated wavelengths for some lines, e.g., for the *Q* branch lines of the (1,1) bandhead and for lines with higher rotational quantum numbers. Such lines are seen in the solar spectrum but their wavelengths are not available from laboratory data. Comparison of observed and computed solar spectra showed that better agreement between them would be obtained by altering a few of the calculated wavelengths by a few hundredths of an Angstrom, and these small changes were consequently made. In addition, we used the *A–X* oscillator strengths ( $f_{00}$ ,  $f_{11}$ , and  $f_{22}$ ) from Larsson & Siegbahn (1983, 1986) instead of values based on Franck–Condon factor calculations.

As before, plane-parallel, flux-constant model atmospheres were computed using the MARCS program (Gustafsson *et al.* 1975). The model atmospheres were then used as input to the SSG program (Bell & Gustafsson 1978, 1989; Gustafsson & Bell 1979) which generated spectra between 3000 and 12 000 Å with a flux point spacing of 0.1 Å. Runs with 0.01 Å spacing were found, in general, to lead to insignificant differences in the final spectral indices (see Sec. 3). Although the improvements to our input data as detailed above were important in matching certain individual absorption features, they had very little effect on the broadband colors. That is, our newly computed isochrone colors and magnitudes still match the color–magnitude diagram of M67 quite nicely (see TDB93, Fig. 2).

Because an important aspect of this paper is to examine the effect of nonsolar abundance ratios, we have recomputed the model atmospheres and synthetic spectra with various element enhancements. New models were run with the abundances of carbon, nitrogen, oxygen, magnesium, iron, calcium, sodium, silicon, chromium, titanium, manganese, nickel, and vanadium each doubled in turn. The effects of the carbon abundance change, which just produces carbon stars, are about twice as great as those caused by using [C/M]=+0.15 at all but the lowest temperatures. An additional sequence was generated where we doubled the abundances for *all* of the metals (i.e., [M/H]=+0.3). Note, however, that all cases were based on the same isochrone, i.e., the  $T_{\text{eff}}$  and  $\log g$  remained fixed. In this way we isolate the abundance effects at a given temperature and surface gravity. Also, we have adopted the same opacity distribution function (ODF) in computing the model atmospheres for the individual element enhancements, with the exception of the [M/H]=+0.3 case where an ODF appropriate for twice the solar metallicity was used. Finally, we ran extra models at three points along the red giant branch to simulate the result of simple mixing (C→N) which is seen to occur in giants (Kjaergaard *et al.* 1982). We have not included this effect in all models

on the giant branch since we do not know how it depends in detail on  $T_{\text{eff}}$  and  $\log g$ ; the three points are simply included as a rough guide to the importance of mixing on the spectral indices.

Our spectrum models have been calculated using a smooth variation in microturbulent velocity with luminosity, ranging from 1.0 km/s for dwarfs to 2.5 km/s for the brightest giants. Because changes in microturbulence can significantly affect some of the spectral indices we have also computed alternate model sequences where the microturbulent velocity has been altered by  $\pm 1$  km/s from the default (luminosity-dependent) value. The impact of these variations on the spectral indices are tabulated in Sec. 3.

### 2.2 Spectral Index Measurement

Prior to measuring the Lick/IDS spectral indices we have taken care to match the characteristics of the IDS spectra as closely as possible. The high-resolution synthetic stellar spectra were first smoothed using a gaussian with FWHM of  $8.2 \text{ \AA}$ , which is typical of the resolution of IDS spectra (G. Worthey, private communication). The smoothed spectra were then resampled at intervals of  $1.25 \text{ \AA}$  to match the IDS pixel spacing. A response function was then applied to simulate the spectral response of the observational system. This function was determined by matching IDS spectra for a number of M67 stars (kindly provided by G. Worthey) with our models for those same objects. Finally, the 21 spectral indices between 4000 and 6400  $\text{\AA}$  discussed by WFGB94 were measured from the synthetic spectra following the definitions in that paper. This set of baseline indices are what are used in the next section to compare with the IDS data and empirical fitting functions.

As discussed by WFGB94, there are unpredictable wavelength shifts and stretches in the IDS spectra. Although the Lick group have done an admirable job in reducing all of their observational material to the same scale, there remains some uncertainty in the spectral resolution and wavelength limits for each index, making it difficult for others to reproduce the Lick system. G. Worthey (private communication) has suggested wavelength offsets for each index based on comparisons between IDS and CCD spectra for specific objects and these have been adopted in making our baseline measurements. However, to estimate the size and direction of any errors caused by the uncertainties in wavelength calibration and spectral resolution we have repeated the index measurements while varying these parameters. We have also tried to gauge the importance of the spectral response function used by repeating the index measurements, first with no correction applied (i.e., leaving the spectra on a true flux scale) and then once again with the continuum removed entirely. In general these variations are of borderline significance because most of the spectral indices are measured over a relatively short wavelength interval. In some cases, however, there is an observationally significant effect. All of these are tabulated in Sec. 3.

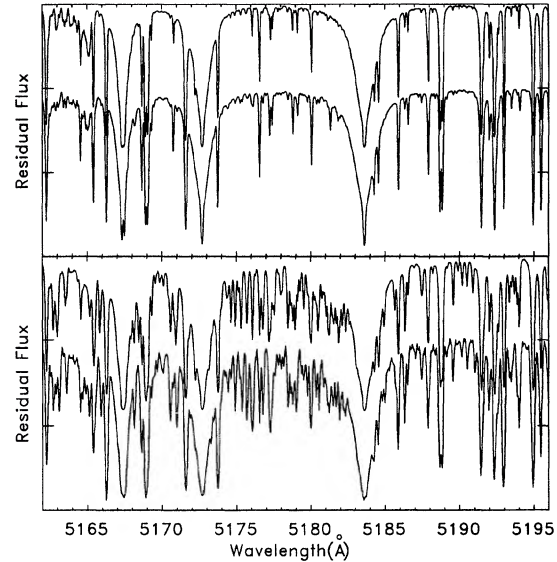


FIG. 1. The synthetic and observed spectra for the wavelength region of the Mg *b* lines are compared for the Sun (upper panel, data from the Kurucz 1984 Atlas) and Arcturus (lower panel, the data being a digital copy of the Griffin 1968 Atlas). The synthetic spectrum is the upper one of each pair. The upper horizontal marking refers to the continuum level of the lower spectrum and the 50% level of the upper spectrum, the lower marking refers to the 50% level of the lower spectrum and the zero level of the upper spectrum.

### 2.3 Matching High-Resolution Spectra of the Sun and Arcturus

The spectral indices derived from synthetic spectra are used here in two distinct ways. On one hand, we use the models to explore the properties of the indices and their sensitivities to various physical and computational parameters. But on the other hand, systematic offsets between observed and predicted indices often serve to point out spectral regions where the models are deficient in some way. Whenever that was evident, we referred to observed high-resolution spectra for the Sun (Kurucz *et al.* 1984) and for Arcturus (Griffin 1968) and made careful line-by-line comparisons with our models for those objects to search for the specific cause of the discrepancy. (Some wavelength regions of the Arcturus atlas were digitized for purposes of these comparisons.) It is very important that we use both a cool giant star and a hotter dwarf in these comparisons because their line spectra look quite different and reflect separate physical conditions. For example, an error in the radiative damping constant for a particular strong line may have a significant impact on its strength and profile in Arcturus while pressure broadening in the Sun dominates and thus camouflages the problem. In addition, molecular lines become much stronger and more important in the spectrum of Arcturus.

Examples of the final fit between the observed and computed spectra for the Sun and Arcturus are given in Fig. 1 and Fig. 2. The former shows the spectral region around the Mg I “*b*” triplet and Mg H (*A–X*) system, while the latter contains the area around the H $\beta$  line. The generally excellent match in Fig. 1 for both strong and weak atomic lines as well

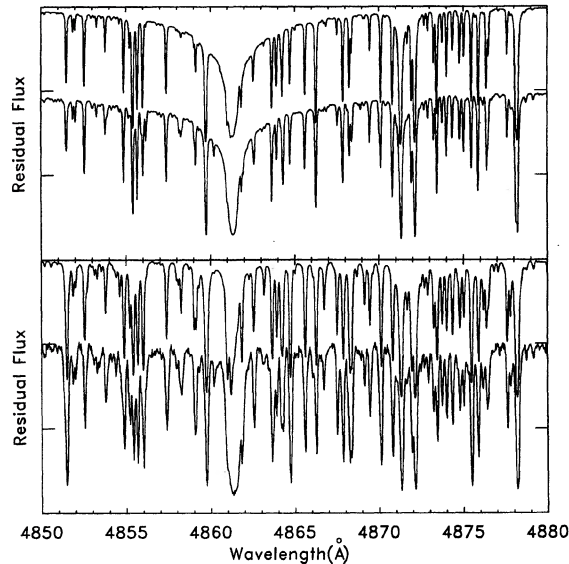


FIG. 2. As Fig. 1, the wavelength region containing the  $H\beta$  line. The weakness of the synthetic  $H\beta$  spectrum for Arcturus is apparent.

as for the complex molecular absorption structure leads one to anticipate good agreement between observed and predicted  $Mg_1$ ,  $Mg_2$ , and  $Mg\ b$  indices. This will in fact be shown to be the case in the following section. Figure 2 demonstrates that while the fit around the  $H\beta$  region is reasonably good for the Sun, the Balmer line itself in the Arcturus model is clearly too weak. But because this line is only a small contributor to the  $H\beta$  index one might expect only a small but noticeable shortfall in the spectral indices for giant stars; this too will be seen in Sec. 3.

While the fits we show to the spectra of the Sun and Arcturus only concern the line spectra, we are also considering the overall fit of our models for these objects to the absolute fluxes (Bell & Tripicco 1996). As noted above, the present work has little dependence on these absolute fluxes.

### 3. RESULTS

Our comparison between theory and observation has two aspects. First, we have chosen 53 stars from the Lick/IDS database. These were chosen on the basis of their tabulated metallicities,  $-0.1 \leq [Fe/H] \leq +0.1$ . Almost all of these are field stars, although there are a few dwarfs from the Coma cluster included. Members of the cluster NGC 188 were excluded on the basis of the sometimes large and unexplained residuals in their indices (WFGB94). All of the M67 stars present in the database are included, since our models are drawn from an isochrone which nicely fits that cluster. (Note that we have included two M67 clump stars in the sample.) A few cool dwarfs whose metallicities are not listed were also included to fill out the sequence at the cool end. The final sample is plotted in the fundamental  $T_{\text{eff}}-\log g$  plane along with the model sequence in Fig. 3. The temperatures used for the stars are those from the Lick/IDS database, which may

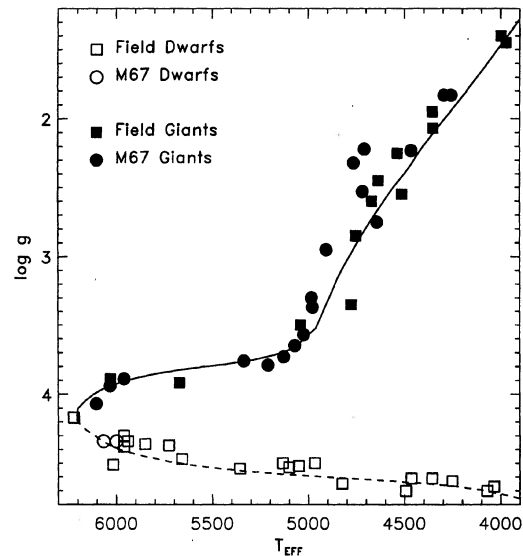


FIG. 3. A 5 Gyr Pop I isochrone, which matches the M67 color-magnitude diagram, is shown as a solid line for post-turnoff stars and a dashed line for pre-turnoff ones.  $T_{\text{eff}}$ ,  $\log g$  points from this isochrone are used as the basis for the index calculations shown in Figs. 4–25. Member stars of M67 are plotted as circles, field stars as squares, filled symbols denoting giants and open ones dwarfs. The same symbols are used in later figures. Two M67 clump stars are included.

differ slightly from those which we would derive from our models.

The second way we compare our model sequence to observation is simply by plugging the model temperatures and gravities (for  $[Fe/H]=0$ ) into the empirical polynomial fitting functions as given in Tables 2 and 3 of WFGB94, thereby projecting our isochrone into spectral index vs. temperature space. The empirical fitting functions have been derived in terms of  $T_{\text{eff}}$ ,  $\log g$ , and  $[Fe/H]$ , using stars of all abundances and assuming that the relative abundances of all elements vary in the same way.

Figures 4–24 show the baseline model sequence (dashed line below the main-sequence turnoff, solid line brighter than the turnoff) compared with the solar abundance stellar sample (filled points for giants and open points for dwarfs) and fitting functions (dot-dashed lines) for each of the 21 spectral indices. An error bar on each plot shows the typical observation  $\pm 1\sigma$  error bar for that index (from WFGB94, Table 1). As discussed above, at three points along the red giant branch (around 4960, 4688, and 4256 K) the carbon and nitrogen abundances have been altered to simulate simple mixing ( $[C/H] \approx -0.2$ ,  $[N/H] \approx +0.4$ ) as observed for Pop I giants (see Tripicco & Bell 1991, and references cited therein). In cases where a spectral index is sensitive to carbon and/or nitrogen abundance these points show up as a “jag” in the model giant branch. Note that such extensive mixing is almost certainly not expected at the base of the RGB and is therefore an overestimate in the case of the 4960 K giant.

Changes to these baseline model spectral index sequences are given in tabular form in terms of the index variations (in units of the typical observational error for that index as given

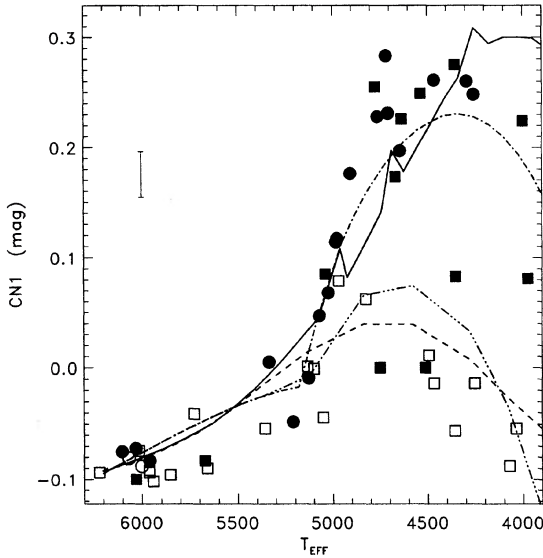


FIG. 4. This diagram shows the  $CN_1$  index plotted vs  $T_{\text{eff}}$ . The symbols are the stars of Fig. 3, while the solid and dashed lines are the isochrone. The jags in the RGB part of the isochrone are caused by three spectra computed with  $[C/Fe]=-0.2$ ,  $[N/Fe]=0.4$ , approximating the abundances seen in Pop I giants by Kjaergaard *et al.* 1982. The remaining lines are the fitting functions of Worthey *et al.* 1994. The preturnoff portion is coded with a single dot-dash line and the post-turnoff portion with a triple dot-dash line. Their estimated rms error for the index is indicated by the errorbar.

by WFGB94). These are listed at three representative points along the model sequence: a cool dwarf ( $T_{\text{eff}} \approx 4575$  K,  $\log g \approx 4.6$ ), a turnoff star ( $T_{\text{eff}} \approx 6200$  K,  $\log g \approx 4.1$ ), and a cool giant ( $T_{\text{eff}} \approx 4255$  K,  $\log g \approx 1.9$ ). Tables 1–3 relate the response of the indices to changes in either the computation of the synthetic spectra (e.g., microturbulent velocity or flux point spacing) or in the measurement of the indices themselves (e.g., smoothing, continuum shape or wavelength off-

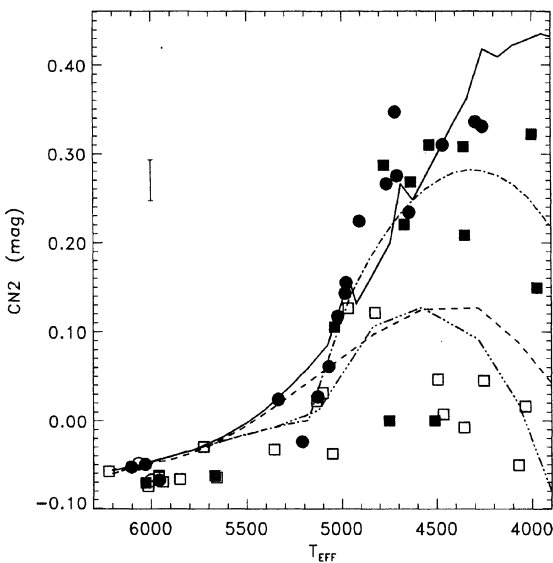


FIG. 5. As Fig. 4, the index being  $CN_2$ .

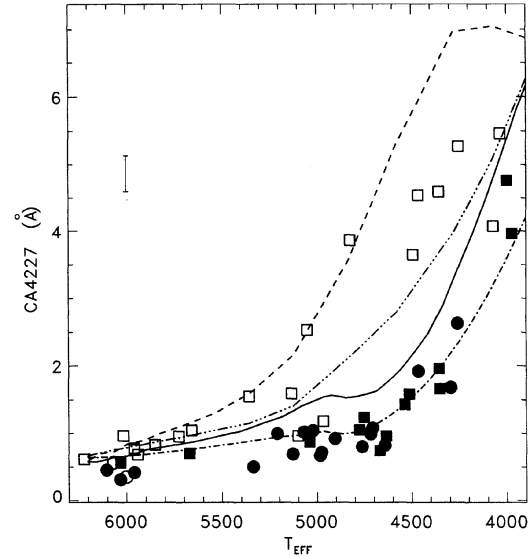


FIG. 6. As Fig. 4, the index being Ca4227.

set). Tables 4–6 quantify the index responses to abundance variations. These tables allow one to see at a glance which spectral indices are most sensitive to the abundance of a particular element or, alternatively, which chemical species dominate a particular index. Three other elements (Mn, V, Ni) were also tested, but found not to affect any of the spectral indices anywhere along the model sequence and so are not included in Tables 4–6. In all of the tables, a positive number indicates that the index increases with the particular quantity while a negative index represents a negative dependence.

#### 4. DISCUSSION

Previous discussions of the effect of changes of abundance and microturbulent velocity on spectral indices and

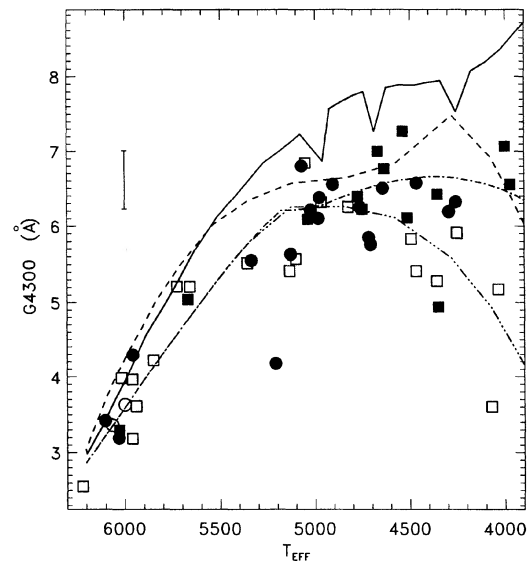


FIG. 7. As Fig. 4, the index being G4300.

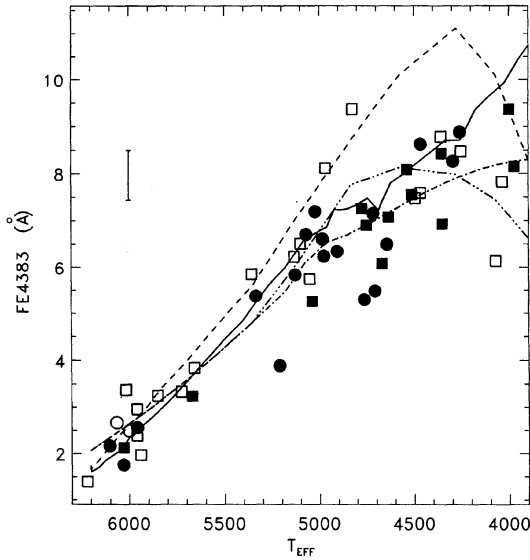


FIG. 8. As Fig. 4, the index being Fe4383.

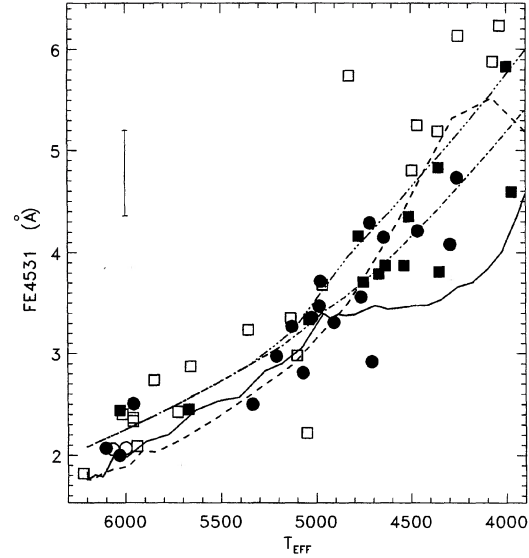


FIG. 10. As Fig. 4, the index being Fe4531.

colors (e.g., Conti & Deutsch 1967) have pointed out that the abundance changes affect primarily the weak lines on the linear part of the curve of growth and the strong lines on the square root part. The lines of intermediate strength, on the flat part of the curve, are much more affected by microturbulent velocity changes than abundance changes. These factors underlie the values shown in the tables, albeit in a complex way. For example, a line which is strong in the spectrum of a cool giant may be intermediate in the spectrum of a hotter dwarf, while changes affect lines in the pseudocontinuum bands as well as the feature bands.

Subsequently, Gustafsson *et al.* (1974; GKA74) measured pairs of narrowband indices in G and K giants. The wavelength interval of one index was chosen so that it contained

lines primarily on the flat part of the curve of growth, the other contained primarily weaker lines. Analysis of this data yielded the microturbulent velocities and abundances of the stars.

From Tables 4–6 it is apparent that the Ca4227, Mg<sub>2</sub>, Mg *b*, and Na D indices, with very strong lines in the feature band, are very dependent upon the abundance of the element forming the dominant line or lines. An overall abundance change produces a smaller change in the index than does the same change in the dominant element, since all the line absorption in the pseudocontinuum bands is affected in the former case and not in the latter. An abundance change causing the introduction of a large number of weak lines, such as the C<sub>2</sub> lines in the feature band of the Fe4668 and Mg<sub>1</sub>

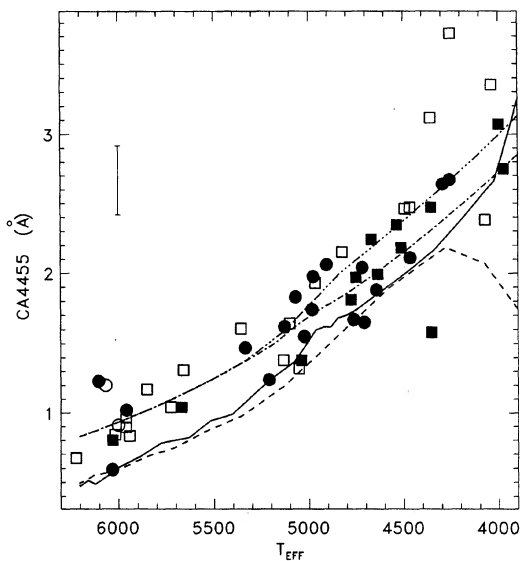


FIG. 9. As Fig. 4, the index being Ca4455.

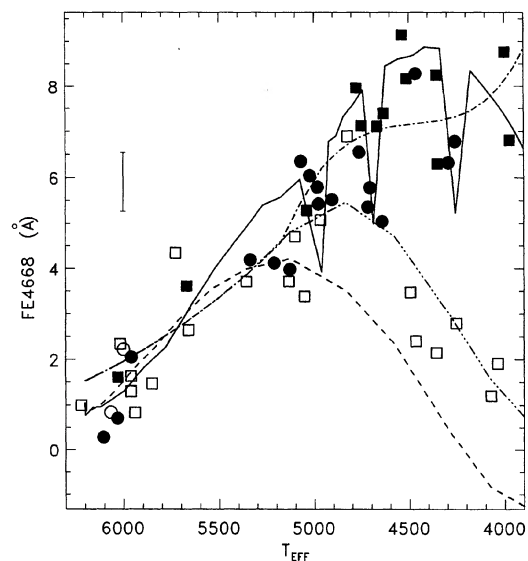
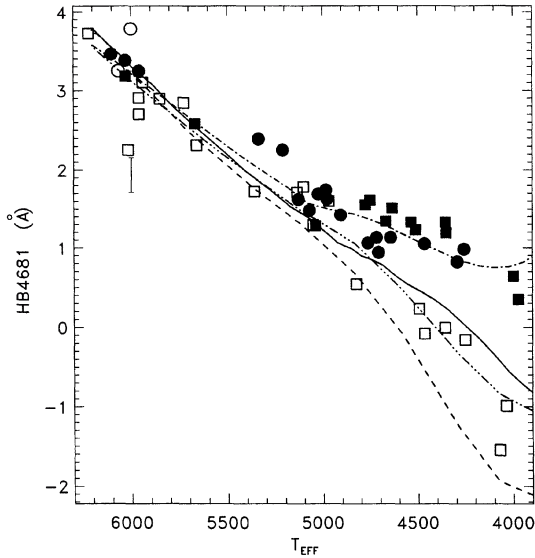


FIG. 11. As Fig. 4, the index being Fe4668.

FIG. 12. As Fig. 4, the index being H $\beta$  4861.

indices, as well as the Mg H lines for the Mg<sub>1</sub> and Mg<sub>2</sub> indices, also has a dramatic effect.

On the other hand, indices formed from feature bands where most of the lines are on the flat part of the curve of growth, such as G4300 and some of the Fe indices, depend on the microturbulent velocity. In fact, in the spectra of the turn off stars and giants which are expected to dominate the light of galaxies, the only Fe index which is more strongly affected by a doubling of the Fe abundance than a doubling of the overall metal abundance is Fe4383. In fact, the results shown in Tables 4 and 5 suggest that it is very difficult to find the abundance of Fe alone from the Lick spectral indices.

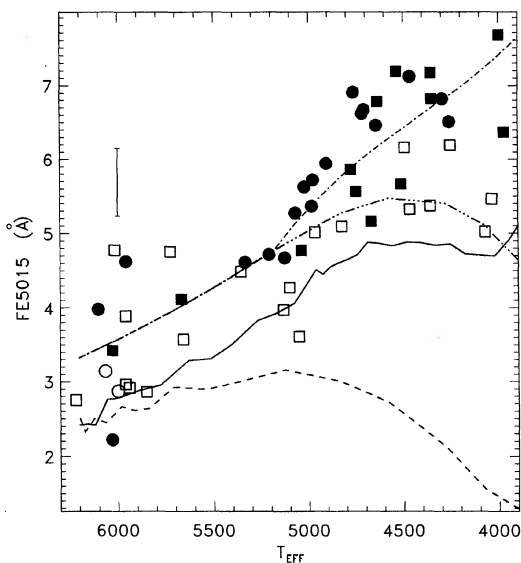
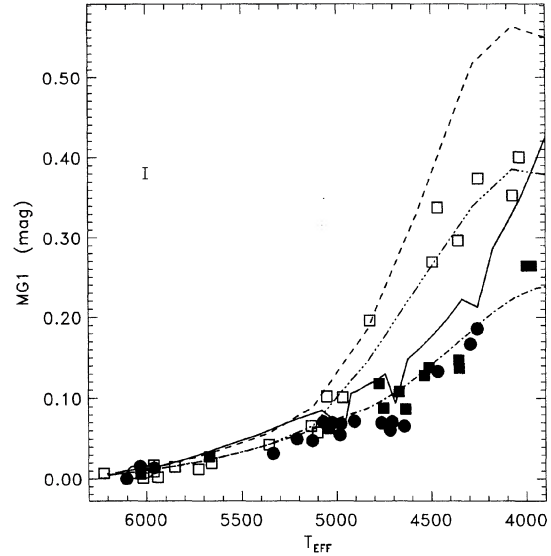
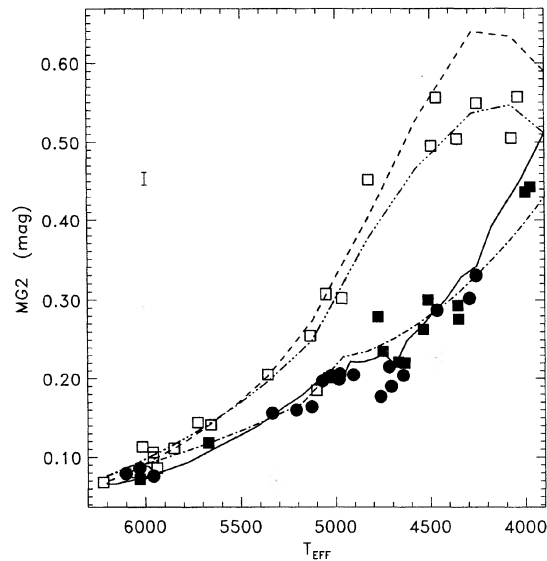


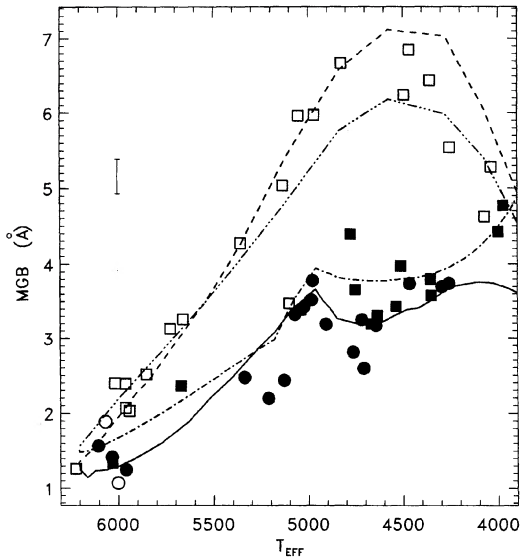
FIG. 13. As Fig. 4, the index being Fe5015.

FIG. 14. As Fig. 4, the index being Mg<sub>1</sub>.

In order to calculate our indices, we have adopted a particular variation of microturbulent velocity with  $T_{\text{eff}}$  and  $\log g$ , the values increasing with decreasing  $\log g$ . This variation is based in part on the results of GKA74. The data in Tables 1–3 allow the reader to check the dependence of the indices on the value chosen. It is clear that some indices (e.g., Fe5270, Fe5335, and Fe5406, for example) are much more dependent on the value of the microturbulence than are others. The fit of these particular indices to the observations in Figs. 17–19 indicates that the values we use are reasonably correct. An error of 1 km/s for the cooler models would displace our calculations by two or three times the standard error, giving a noticeably poorer fit.

CN<sub>1</sub>, CN<sub>2</sub>.—These indices measure the strength of the

FIG. 15. As Fig. 4, the index being Mg<sub>2</sub>.

FIG. 16. As Fig. 4, the index being Mg *b*.

CN  $\lambda$ 4150 absorption band and differ only in the placement of the blue pseudocontinuum band. Figures 4 and 5 show the model sequences to match the observations quite well, particularly in the divergence of dwarfs and giants. The coolest giant models appear to systematically overestimate the indices, but this is not very surprising given the strong dependence of the CN indices on the abundances of carbon, nitrogen, and oxygen and the uncertainties in the degree and type of internal mixing expected in evolved stars. In addition, Tables 1–3 show that these two indices are among the most sensitive to continuum shape (since they are near the blue end of the IDS range) and to the flux point spacing used in computing the models (presumably due to the large number of weak CN lines which make up the absorption band).

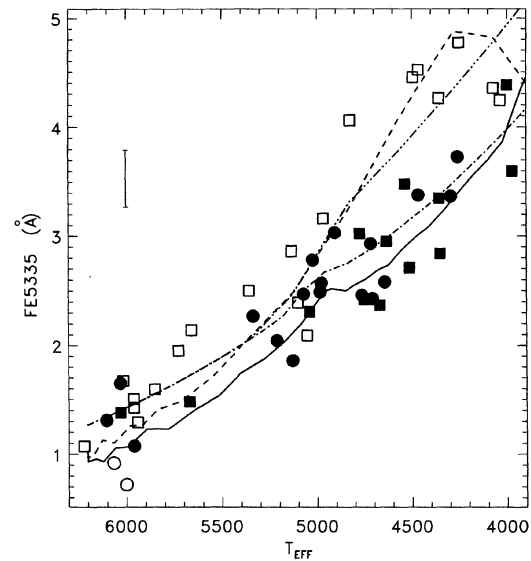


FIG. 18. As Fig. 4, the index being Fe5335.

Ca4227.—The model sequence is systematically high compared to most of the stars in the sample and especially compared to the fitting function for the giants. There are a number of possible explanations, since this index is quite sensitive to bandpass placement and to spectral resolution (Tables 1–3, cols 6–9). However, a more likely reason is that the models were calculated with a combination of Ca abundance and *gf* value which are slightly too high, by about 0.2 dex. As column 9 of Tables 4–6 shows, the Ca4227 index is quite sensitive to calcium abundance and a reduction of 0.2 dex should reduce the index by 0.6–0.7 Å in the cool stars.

G4300.—This index is, as expected, very sensitive to the abundances of carbon and oxygen. This can be seen in the

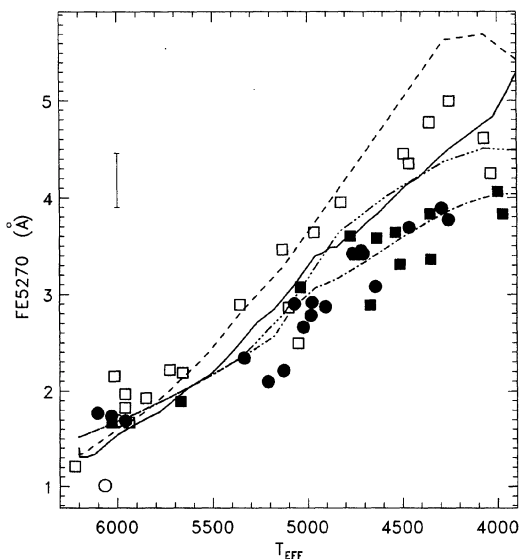


FIG. 17. As Fig. 4, the index being Fe5270.

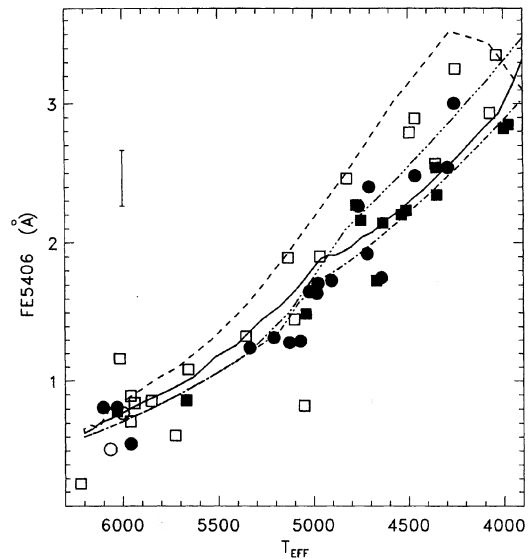


FIG. 19. As Fig. 4, the index being Fe5406.

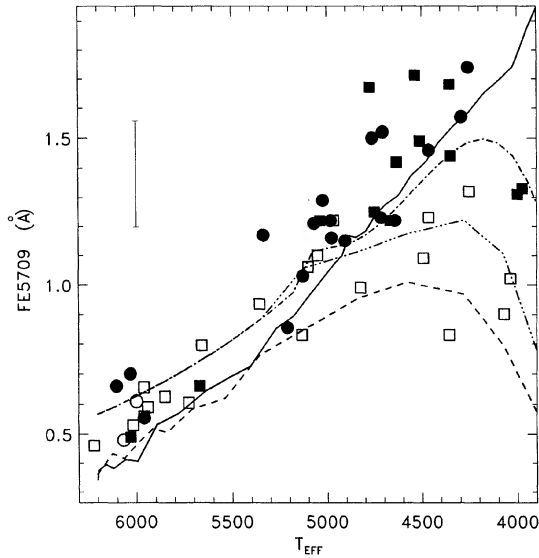


FIG. 20. As Fig. 4, the index being Fe5709.

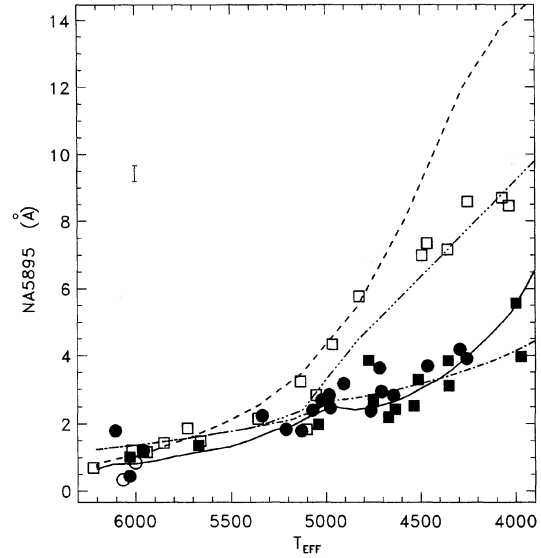


FIG. 22. As Fig. 4, the index being Na5895.

RGB “jags” representing the (C→N) mixed models, as well as in columns 4 and 6 of Tables 4–6. Note that there is also significant sensitivity to Ti abundance and, to a lesser extent, Fe. The coolest giant models continue to rise while the observations stay flat or turn down. This may again tell us something about the progression of mixing along the RGB.

Fe4383.—As expected, iron is the dominant chemical species in this index. Carbon and magnesium also affect the strength. Tables 1–3 indicate a significant dependence on the microturbulent velocity used in computing the synthetic spectra. This index shows the greatest dependence of all the Fe indices on a change in iron abundance as opposed to a change in overall metal abundance. This must occur because of the strength of the  $\lambda 4383$  line of Fe itself, since its

strength is comparable to that of the Mg *b* and Na D lines.

Ca4455.—While there is a small systematic offset between the models and observations for this index, Tables 1–3 reveal strong dependence on the bandpass placement which could account for it. Perhaps the most interesting feature about Ca4455 is that it is nearly insensitive to the abundance of calcium! In fact, the index displays very little variation with respect to any single element or to overall metallicity. The dominant contributors appear to be Fe and Cr.

Fe4531.—The abundance of Ti dominates the behavior of this index. The fit between the models and observations is quite good throughout.

Fe4668.—The extreme displacement of the mixed giant branch models with respect to the unmixed sequence in Fig.

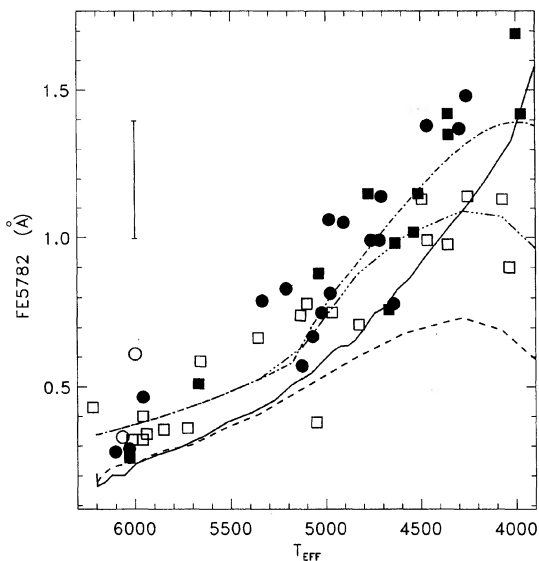
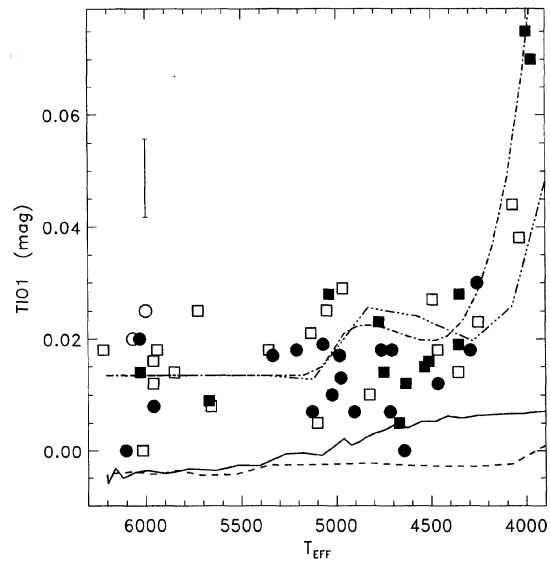
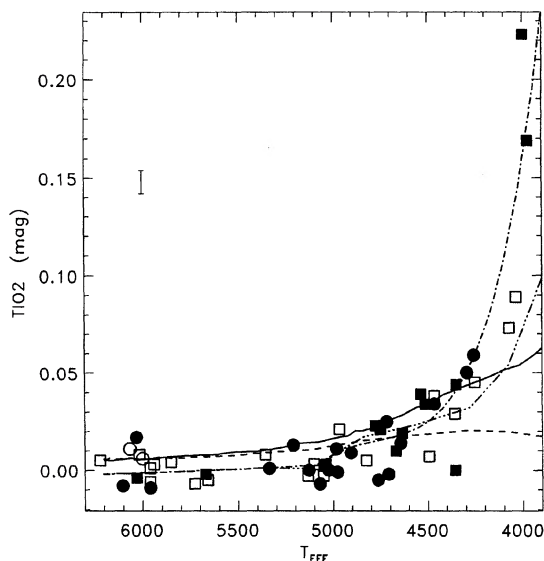


FIG. 21. As Fig. 4, the index being Fe5782.

FIG. 23. As Fig. 4, the index being TiO<sub>1</sub>.

FIG. 24. As Fig. 4, the index being  $\text{TiO}_2$ .

11 hints at the extraordinary sensitivity which this index has to carbon abundance. This is due to the  $\Delta\nu=1$  Swan bands of  $\text{C}_2$  which blanket the feature bandpass. Tables 4–6 reveal there to be only a weak dependence on iron abundance. We expand on the behavior of this index in Fig. 25, where we plot the entire model sequence for enhanced oxygen, iron,

overall metallicity and finally for carbon. Because doubling carbon pushes its abundance slightly beyond that of oxygen (thus creating carbon stars) we have also included an extra sequence where  $[\text{C}/\text{H}]=+0.15$ . Note how the Fe-enhanced sequence barely differs from the baseline sequence. However, the carbon-enhanced sequences jump up sharply while the oxygen-enhanced models cause the index to drop significantly (since the extra oxygen ties up more of the carbon in CO).

This dependence of Fe4668 on carbon abundance may have important observational consequences since Luck & Challener (1995) have suggested that the strong CN bands in strong line stars such as  $\mu$  Leo are caused by  $[\text{C}/\text{Fe}]\approx 0.1$ . Since they deduce their carbon abundance from  $\text{C}_2$  lines, it is apparent that this index will give unreliable results for metal-rich stars with  $[\text{C}/\text{Fe}]\approx 0.1$ . While Luck & Challener estimate such metal-rich stars are rare in our Galaxy, being perhaps 15% of the total, this number is uncertain and such stars maybe more prevalent in other galaxies.

Since this index is so dependent on C abundance and depends very weakly on Fe abundance, it might well be re-named.

$\text{H}\beta$ .—The agreement between theory and observation is quite good for this index for temperatures above 5100 K. At cooler temperatures the models are systematically too weak for the  $\text{H}\beta$  line itself (see Fig. 2), owing to neglect of non-LTE effects. Though there are many other lines in the feature bandpass, Tables 4–6 indicate that there is very little metal-

TABLE 1. Spectral index response: Cool dwarf (4575/4.6).

(1)	(2)	(3)	(4)	(5)	(6)	(7)	(8)	(9)	(10)	(11)	(12)
			Microturbulence		Offset		FWHM		Continuum		Resolution
Index	$I_0$	Error	+1 km/s	-1 km/s	+3Å	-3Å	10.2Å	6.2Å	Flat	Flux	0.01Å/pt
CN <sub>1</sub>	0.04	0.021	1.0	-0.3	0.1	-0.8	-0.3	0.4	1.2	1.0	1.1
CN <sub>2</sub>	0.12	0.023	1.5	-0.5	0.5	-2.4	-0.9	0.9	1.7	1.5	1.0
Ca4227	5.33	0.270	1.7	-1.2	0.7	-5.7	-1.9	1.7	-0.0	0.0	0.2
G4300	6.83	0.390	0.8	-0.4	1.0	-1.3	-0.1	0.4	-0.4	-0.3	-0.8
Fe4383	10.09	0.530	4.2	-2.5	1.0	-5.4	-1.0	0.8	0.1	0.0	0.1
Ca4455	1.89	0.250	1.9	-1.2	6.3	-8.0	-1.1	1.2	-0.1	-0.1	0.3
Fe4531	4.28	0.420	1.6	-0.8	1.3	-3.8	-0.6	0.6	0.1	0.1	0.2
Fe4668	2.34	0.640	0.4	-0.1	-0.1	-0.5	-0.2	0.1	0.5	0.5	-0.3
H $\beta$	-0.10	0.220	-0.6	0.3	-2.1	3.2	0.0	-0.0	0.1	0.1	-0.3
Fe5015	2.72	0.460	1.6	-1.2	0.9	-4.9	-0.9	1.1	0.2	0.1	-0.1
Mg <sub>1</sub>	0.33	0.007	2.6	-1.5	-0.1	-0.6	-0.4	0.3	-1.0	-1.4	-0.2
Mg <sub>2</sub>	0.53	0.008	5.2	-2.6	1.0	-2.3	-0.3	0.5	-0.9	-1.4	-0.7
Mg b	7.12	0.230	1.1	-0.6	-0.2	-1.9	-1.1	0.8	0.1	-0.0	-0.6
Fe5270	4.79	0.280	2.4	-1.3	-2.7	-0.5	-0.9	0.9	-0.2	-0.1	-0.0
Fe5335	4.05	0.260	3.5	-2.0	-3.3	-1.2	-1.4	1.2	-0.0	-0.0	0.1
Fe5406	3.01	0.200	1.9	-1.1	-1.4	-1.4	-1.5	1.2	0.0	-0.0	-0.5
Fe5709	1.01	0.180	0.9	-0.6	0.1	-1.0	-0.2	0.2	-0.0	-0.0	-0.1
Fe5782	0.68	0.200	0.5	-0.2	0.0	-1.0	-0.3	0.2	-0.0	-0.0	-0.2
Na D	8.11	0.240	3.4	-1.6	-0.7	-0.4	-0.4	0.3	0.0	0.0	0.2
TiO <sub>1</sub>	-0.00	0.007	0.4	-0.3	0.5	-0.5	-0.0	-0.0	0.7	0.6	0.1
TiO <sub>2</sub>	0.02	0.006	0.6	-0.4	0.4	-0.5	-0.0	0.0	-0.5	-0.5	-0.2

Notes to Table 1.

Column 2 gives the computed index value, column 3 gives the (observed) standard error, and columns 4–12 give the effect of the changes in units of the standard error.

TABLE 2. Spectral index response<sup>a</sup>: Turnoff star (6200/4.1).

(1)	(2)	(3)	(4)	(5)	(6)	(7)	(8)	(9)	(10)	(11)	(12)
Index	I <sub>0</sub>	Error	Microturbulence		Offset		FWHM		Continuum		Resolution 0.01Å/pt
			+1 km/s	-1 km/s	+3Å	-3Å	10.2Å	6.2Å	Flat	Flux	
CN <sub>1</sub>	-0.09	0.021	0.2	-0.1	-0.6	0.1	-0.1	0.1	0.0	-0.1	-0.0
CN <sub>2</sub>	-0.06	0.023	0.3	-0.1	0.1	-1.0	-0.3	0.3	0.2	0.1	0.2
Ca4227	0.58	0.270	0.4	-0.2	0.0	-0.7	-0.3	0.2	0.0	0.0	0.2
G4300	2.98	0.390	1.4	-0.5	0.5	-1.4	-0.4	0.4	0.1	0.1	-0.2
Fe4383	1.61	0.530	1.2	-0.8	0.4	-1.6	-0.3	0.2	0.1	-0.1	0.2
Ca4455	0.47	0.250	1.4	-1.2	1.7	-1.8	-0.2	0.3	0.1	-0.0	0.6
Fe4531	1.76	0.420	1.6	-0.9	-0.1	-0.8	-0.3	0.3	0.1	0.1	0.4
Fe4668	0.77	0.640	0.3	-0.1	0.3	-0.5	-0.0	0.0	0.5	0.5	0.4
Hβ	3.79	0.220	0.1	-0.2	-0.7	0.1	-0.3	0.2	0.0	0.0	0.2
Fe5015	2.42	0.460	2.0	-1.1	-0.1	-1.2	-0.3	0.4	-0.0	0.0	0.2
Mg <sub>1</sub>	0.01	0.007	0.3	-0.1	0.0	-0.0	-0.0	0.0	-0.8	-0.8	0.4
Mg <sub>2</sub>	0.07	0.008	1.0	-0.6	-0.2	0.2	-0.1	0.1	-0.9	-0.9	-0.1
Mg b	1.25	0.230	0.6	0.0	-1.3	0.8	-0.3	0.2	-0.2	-0.0	0.1
Fe5270	1.31	0.280	1.1	-0.7	-1.2	0.2	-0.2	0.2	-0.1	-0.0	-0.0
Fe5335	0.93	0.260	0.8	-0.4	-0.1	-0.9	-0.4	0.3	0.1	-0.0	-0.0
Fe5406	0.63	0.200	0.3	-0.2	-0.6	0.1	-0.2	0.2	0.2	-0.0	-0.4
Fe5709	0.37	0.180	0.7	-0.3	0.1	-0.3	-0.1	0.0	-0.0	-0.0	0.3
Fe5782	0.16	0.200	-0.0	0.0	-0.1	-0.2	-0.1	0.1	0.2	-0.0	0.0
Na5895	0.66	0.240	0.4	-0.1	-0.3	0.3	-0.0	0.1	0.4	0.0	0.4
TiO <sub>1</sub>	-0.01	0.007	0.2	-0.2	0.1	-0.1	-0.0	-0.0	0.9	0.7	0.4
TiO <sub>2</sub>	0.01	0.006	0.0	-0.2	0.2	-0.3	-0.0	0.0	-0.4	-0.3	-0.1

<sup>a</sup>see note to Table 1TABLE 3. Spectral index response<sup>a</sup>: Cool giant (4255/1.9).

(1)	(2)	(3)	(4)	(5)	(6)	(7)	(8)	(9)	(10)	(11)	(12)
Index	I <sub>0</sub>	Error	Microturbulence		Offset		FWHM		Continuum		Resolution 0.01Å/pt
			+1 km/s	-1 km/s	+3Å	-3Å	10.2Å	6.2Å	Flat	Flux	
CN <sub>1</sub>	0.28	0.021	0.7	-2.5	-0.5	-0.6	-0.3	0.4	0.6	0.4	-1.0
CN <sub>2</sub>	0.39	0.023	0.8	-3.1	-0.2	-1.9	-0.9	0.9	1.3	0.9	-1.7
Ca4227	3.39	0.270	1.1	-1.3	-0.7	-3.4	-1.6	1.4	-0.0	-0.0	0.4
G4300	8.00	0.390	2.0	-1.4	0.7	-1.5	-0.3	0.5	-0.4	-0.3	-0.3
Fe4383	9.02	0.530	1.7	-3.0	-0.3	-3.5	-1.1	0.9	-0.1	-0.1	-0.9
Ca4455	2.28	0.250	2.5	-3.7	1.4	-4.2	-1.2	1.2	-0.0	-0.0	-0.9
Fe4531	3.59	0.420	2.3	-2.2	1.6	-3.6	-0.4	0.4	0.2	0.1	1.1
Fe4668	8.62	0.640	0.3	-0.7	-0.1	-0.9	-0.3	0.2	0.4	0.3	-0.7
Hβ	0.05	0.220	1.4	0.6	-1.7	3.0	0.1	0.0	0.0	0.0	0.6
Fe5015	4.79	0.460	2.9	-3.5	-0.3	-3.3	-1.0	1.1	0.1	0.1	-0.6
Mg <sub>1</sub>	0.25	0.007	2.2	-2.7	-0.7	0.1	-0.3	0.3	-1.1	-1.5	0.4
Mg <sub>2</sub>	0.36	0.008	2.9	-3.2	0.6	-1.7	-0.2	0.3	-1.1	-1.5	-0.7
Mg b	3.65	0.230	-0.5	0.3	0.2	-1.4	-0.6	0.4	-0.1	-0.0	-0.8
Fe5270	4.49	0.280	2.3	-2.8	-0.5	-1.9	-0.9	0.9	-0.2	-0.1	-0.4
Fe5335	3.40	0.260	3.4	-3.2	-2.8	-1.4	-1.3	1.2	-0.0	-0.0	0.2
Fe5406	2.60	0.200	3.0	-1.1	0.4	-2.8	-1.2	1.0	0.0	-0.0	0.4
Fe5709	1.59	0.180	1.7	-1.9	0.4	-1.9	-0.4	0.4	-0.0	-0.0	-0.1
Fe5782	1.12	0.200	1.3	-0.7	0.0	-1.8	-0.5	0.4	0.0	-0.0	0.0
Na D	3.93	0.240	2.4	-2.3	-0.7	-0.0	-0.3	0.3	0.1	0.0	0.2
TiO <sub>1</sub>	0.01	0.007	0.1	-1.0	0.4	-0.4	-0.0	-0.0	0.7	0.5	-0.3
TiO <sub>2</sub>	0.05	0.006	1.8	-1.3	0.3	-0.6	-0.1	0.0	-0.5	-0.5	0.0

<sup>a</sup>see note to Table 1

TABLE 4. Spectral index response to abundance changes: Cool dwarf (4575/4.6).

(1)	(2)	(3)	(4)	(5)	(6)	(7)	(8)	(9)	(10)	(11)	(12)	(13)	(14)
Index	$I_0$	Error	C	N	O	Mg	Fe	Ca	Na	Si	Cr	Ti	[M/H]
CN <sub>1</sub>	0.04	0.021	7.9	1.5	-1.4	-0.2	-0.2	-0.4	-0.1	1.3	-1.2	0.2	0.5
CN <sub>2</sub>	0.12	0.023	7.6	1.5	-1.5	-0.5	-0.1	-0.4	-0.2	1.9	-1.1	0.3	0.8
Ca4227	5.33	0.270	-3.5	-0.4	0.7	-0.2	-0.1	3.9	-0.2	-0.2	-0.3	0.1	1.7
G4300	6.83	0.390	6.8	0.0	-2.0	-0.5	-1.1	0.7	-0.2	0.2	-0.2	1.7	0.6
Fe4383	10.09	0.530	1.4	0.1	-0.1	-1.5	5.3	-1.0	-0.4	-0.8	-0.2	0.3	1.2
Ca4455	1.89	0.250	-0.3	-0.0	0.1	-0.3	-0.5	0.2	-0.1	-0.3	0.6	0.2	0.8
Fe4531	4.28	0.420	-0.6	0.0	0.1	-0.8	0.7	-0.0	0.0	-0.9	0.5	2.0	1.2
Fe4668	2.34	0.640	14.4	-0.0	-1.1	-0.3	0.8	0.2	0.0	-1.2	-0.4	0.3	1.1
H $\beta$	-0.10	0.220	0.2	0.1	-0.1	-1.6	0.0	0.0	0.1	0.2	-0.3	-0.5	-0.7
Fe5015	2.72	0.460	0.1	0.2	0.1	-2.7	0.9	0.0	0.1	0.0	-0.0	2.5	0.9
Mg <sub>1</sub>	0.33	0.007	12.4	-0.1	-1.0	14.6	-4.4	-1.6	-1.2	-1.1	-0.8	1.5	4.2
Mg <sub>2</sub>	0.53	0.008	6.2	0.1	-0.6	12.2	-2.8	-1.1	-1.1	-0.9	-0.7	1.6	4.8
Mg <i>b</i>	7.12	0.230	0.8	0.2	0.1	6.3	-1.3	-0.3	-0.6	-0.1	-2.2	0.4	1.5
Fe5270	4.79	0.280	0.1	-0.0	-0.1	-1.1	2.8	0.7	-0.1	-0.3	-0.1	0.3	1.6
Fe5335	4.05	0.260	-0.4	0.0	0.1	-1.1	3.0	-0.2	-0.3	-0.3	1.0	0.5	1.7
Fe5406	3.01	0.200	0.1	0.0	0.0	-1.0	3.0	-0.2	-0.3	-0.2	0.5	0.2	1.5
Fe5709	1.01	0.180	-0.5	-0.0	0.0	-0.0	0.7	-0.0	-0.4	-0.1	0.2	0.3	0.8
Fe5782	0.68	0.200	0.1	-0.0	0.1	0.0	-0.1	-0.1	-0.0	0.0	0.8	-0.0	0.7
Na D	8.11	0.240	-0.1	0.1	0.1	-1.1	-0.5	-0.6	7.6	-0.1	-0.1	0.5	4.6
TiO <sub>1</sub>	-0.00	0.007	1.1	0.1	-0.0	-0.0	0.0	-0.0	-0.0	0.0	-0.0	0.2	0.0
TiO <sub>2</sub>	0.02	0.006	0.9	-0.0	0.1	-0.1	0.5	-0.4	-0.1	0.0	-0.0	0.2	0.6

Notes to Table 4.

Column 2 gives the computed index value, column 3 gives the (observed) standard error, columns 4–13 give the effect of the changes in units of the standard error as the element abundance is increased by 0.3 dex, and column 14 gives the effect (again in units of the standard error) for an increase in *overall* metallicity by 0.3 dex

TABLE 5. Spectral index response<sup>a</sup> to abundance changes: Turnoff star (6200/4.1).

(1)	(2)	(3)	(4)	(5)	(6)	(7)	(8)	(9)	(10)	(11)	(12)	(13)	(14)
Index	$I_0$	Error	C	N	O	Mg	Fe	Ca	Na	Si	Cr	Ti	[M/H]
CN <sub>1</sub>	-0.09	0.021	-0.1	0.3	0.0	0.1	0.1	-0.1	-0.1	-0.1	-0.0	0.0	0.0
CN <sub>2</sub>	-0.06	0.023	-0.1	0.3	0.0	0.0	0.1	-0.1	-0.1	0.0	-0.0	0.0	0.2
Ca4227	0.58	0.270	-0.3	-0.1	0.1	0.0	0.4	0.5	-0.1	0.1	-0.1	-0.0	0.6
G4300	2.98	0.390	3.1	0.0	-0.0	-0.5	-0.3	0.1	-0.1	-0.7	-0.2	0.4	0.8
Fe4383	1.61	0.530	0.8	0.1	0.0	0.1	0.9	-0.4	-0.3	-0.1	0.1	0.4	1.0
Ca4455	0.47	0.250	0.0	-0.0	0.0	-0.0	0.0	-0.0	0.0	0.1	0.2	-0.1	0.7
Fe4531	1.76	0.420	0.1	0.0	0.1	-0.0	0.3	-0.0	0.0	-0.0	0.2	0.3	0.7
Fe4668	0.77	0.640	2.4	-0.1	0.0	-0.1	0.4	-0.1	0.1	-0.2	-0.1	0.2	1.6
H $\beta$	3.79	0.220	0.1	0.0	0.1	0.1	-0.2	0.0	0.2	0.1	-0.2	0.2	0.5
Fe5015	2.42	0.460	-0.1	-0.0	-0.2	-0.1	0.5	0.0	0.1	-0.3	-0.4	0.1	1.1
Mg <sub>1</sub>	0.01	0.007	3.4	0.1	-0.1	0.2	-0.5	0.1	-0.2	-0.4	-0.2	0.1	1.2
Mg <sub>2</sub>	0.07	0.008	1.1	-0.2	0.1	2.0	-0.2	0.3	0.2	-0.7	-0.2	0.1	1.7
Mg <i>b</i>	1.25	0.230	-0.5	-0.3	-0.2	2.4	-0.4	0.2	0.3	-0.6	-0.3	-0.4	0.5
Fe5270	1.31	0.280	0.1	0.1	0.2	-0.1	0.7	0.5	-0.1	0.2	0.1	0.3	1.3
Fe5335	0.93	0.260	0.1	0.0	0.0	-0.2	1.0	0.1	0.0	0.2	0.1	0.2	0.6
Fe5406	0.63	0.200	0.3	0.2	0.1	0.3	0.9	-0.2	-0.2	0.2	0.6	0.3	1.1
Fe5709	0.37	0.180	-0.0	0.0	-0.0	0.1	0.6	0.1	-0.2	-0.0	0.1	0.1	0.6
Fe5782	0.16	0.200	0.2	0.3	0.1	0.1	0.1	-0.2	-0.2	0.2	0.5	0.2	0.7
Na D	0.66	0.240	0.4	0.5	0.5	0.2	0.1	-0.4	0.4	0.2	0.7	0.4	0.9
TiO <sub>1</sub>	-0.01	0.007	-0.1	0.5	0.2	0.3	0.2	-0.1	-0.4	0.0	0.1	0.4	0.0
TiO <sub>2</sub>	0.01	0.006	-0.2	0.2	-0.1	0.1	0.4	-0.0	0.1	-0.1	0.0	-0.0	0.1

<sup>a</sup>see note to Table 4

TABLE 6. Spectral index response<sup>a</sup> to abundance changes: Cool giant (4255/1.9).

(1)	(2)	(3)	(4)	(5)	(6)	(7)	(8)	(9)	(10)	(11)	(12)	(13)	(14)
Index	$I_0$	Error	C	N	O	Mg	Fe	Ca	Na	Si	Cr	Ti	[M/H]
CN <sub>1</sub>	0.28	0.021	14.6	4.3	-3.9	-1.2	-0.4	-0.5	-0.2	1.0	-0.8	0.3	3.4
CN <sub>2</sub>	0.39	0.023	14.1	4.3	-3.8	-1.4	-0.5	-0.6	-0.2	1.5	-0.7	0.4	3.7
Ca4227	3.39	0.270	-4.5	-0.8	1.5	0.1	0.5	4.3	-0.1	-0.0	-0.1	-0.0	3.2
G4300	8.00	0.390	4.6	0.1	-1.6	-0.3	-0.8	0.3	-0.2	0.3	-0.4	1.2	0.6
Fe4383	9.02	0.530	1.1	-0.1	-0.4	-1.1	3.1	-0.4	-0.1	-0.7	-0.0	0.2	1.7
Ca4455	2.28	0.250	-0.6	-0.1	0.1	-0.1	-0.9	0.0	-0.1	-0.1	0.6	0.4	1.2
Fe4531	3.59	0.420	0.0	0.2	0.1	-0.1	0.2	-0.0	0.1	-0.6	0.4	1.1	1.2
Fe4668	8.62	0.640	25.2	0.1	-4.0	-0.9	0.1	-0.1	-0.2	-1.6	-0.2	0.5	4.0
H $\beta$	0.05	0.220	0.4	-0.0	-0.1	-0.7	0.3	-0.0	0.0	0.1	-0.4	-0.1	-0.4
Fe5015	4.79	0.460	0.0	-0.0	0.1	-1.4	1.0	0.1	0.1	-0.2	-0.0	1.1	1.2
Mg <sub>1</sub>	0.25	0.007	26.1	-0.2	-4.1	9.1	-3.1	-0.6	-0.4	-1.6	-0.3	0.7	6.7
Mg <sub>2</sub>	0.36	0.008	4.9	-0.1	-1.7	10.4	-2.3	-0.5	-0.4	-1.3	-0.4	0.9	6.1
Mg <i>b</i>	3.65	0.230	-3.5	0.0	0.1	6.0	-1.3	-0.2	-0.4	-0.4	-2.0	0.1	1.3
Fe5270	4.49	0.280	1.4	0.3	-0.2	-0.9	1.7	0.1	-0.1	-0.3	0.1	0.2	1.8
Fe5335	3.40	0.260	-1.0	-0.1	0.1	-0.6	2.4	-0.0	-0.1	-0.2	0.5	0.2	1.9
Fe5406	2.60	0.200	0.3	0.1	-0.1	-0.5	2.0	-0.1	-0.1	-0.2	0.4	0.1	1.5
Fe5709	1.59	0.180	-1.1	-0.1	0.1	0.1	0.5	-0.0	-0.2	-0.0	0.2	0.3	1.2
Fe5782	1.12	0.200	-0.2	-0.0	0.0	0.0	0.0	-0.0	-0.0	0.1	1.0	-0.2	1.1
Na D	3.93	0.240	1.0	0.3	-0.1	-0.7	-0.2	-0.2	4.3	-0.2	0.0	0.2	4.1
TiO <sub>1</sub>	0.01	0.007	2.8	0.5	-0.5	-0.1	-0.3	-0.0	0.0	-0.2	-0.1	0.0	0.2
TiO <sub>2</sub>	0.05	0.006	5.8	0.7	-0.5	-0.2	0.5	-0.2	0.1	-0.2	-0.1	0.1	1.1

<sup>a</sup>see note to Table 4

licity sensitivity in the H $\beta$  index. In fact it is the only index where an increase in overall metallicity causes the index to drop. The dominant metal appears to be Mg, probably via Mg H absorption in the pseudocontinuum bands.

Fe5015.—This is arguably the poorest fit we have encountered between the model sequences and the observations. The model sequence is systematically too low by  $\approx 1$

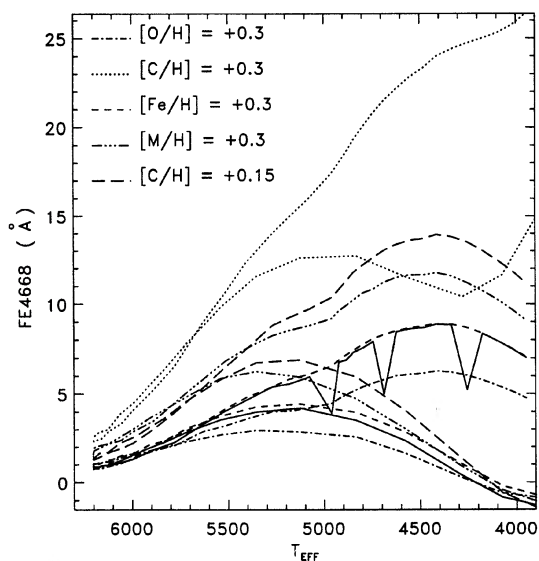


FIG. 25. The values of the Fe4668 index, plotted vs  $T_{\text{eff}}$ , are shown for a number of different chemical compositions as coded in the figure legend. [M/H] refers to overall metallicity, while [X/H] in the other cases refers to element X only.

Å for reasons we have not been able to determine. The fit of our synthetic solar spectrum to the observational data in the wavelength region of this index is as good as it is in other wavelength regions. The dominant metals are Ti and Mg and they operate in opposite directions.

Mg<sub>1</sub>, Mg<sub>2</sub>, Mg *b*.—These are among the most important and widely used of the Lick/IDS indices and so it is gratifying to see how nicely the model sequences fit the observations in Figs. 14–16. Examination of Tables 4–6 shows how complicated these indices are: while they are, of course, very sensitive to Mg abundance they also depend strongly on carbon (again through the C<sub>2</sub> Swan bands), iron and several other species. In fact, there is even a dependence on Mg isotope ratio for the cooler objects.

Fe5270, Fe5335, Fe5406.—These three iron indices are quite similar and all are fitted well by the models. Fe is by far the dominant contributor to the metallicity sensitivity.

Fe5709.—This index is also nicely fitted by the models, but Tables 4–6 show that the overall metallicity sensitivity is lower than the three previous Fe indices. This is probably caused by the small positive dependence on Fe being balanced by the nearly equal negative sensitivity to carbon.

Fe5782.—The model sequence is somewhat low systematically, but the observational error bar (Fig. 21) is large. The only element which seems to affect this index significantly is Cr. The index is nearly independent of Fe.

Na D.—The agreement between theory and observation is quite good for this index except for the coolest dwarfs, for which the models seem to predict values which are too high. The dominant element here is, unsurprisingly, Na.

TiO<sub>1</sub>, TiO<sub>2</sub>.—While we have modeled these indices, we have not included TiO lines in our current models, and so we expect to see the model predictions falling far short of the observations as temperatures approach 4000 K. However, these diagrams should provide excellent guidance as we refine our TiO linelist and reimplement this species, which dominates the spectra of M stars.

## 5. CONCLUSIONS

As stated earlier, this paper was written in part to check our calculations of the Lick indices, in part to see where our initial calculations needed improvement for this specific purpose and in part to see how change in the abundances of particular species would affect the synthetic indices.

Our initial calculations were based on the N line list used by Bell *et al.* (1994). These authors have compared synthetic and observed solar spectra over the wavelength range 3000–12 000 Å and give examples of the fits which they have obtained. We carried out some further improvements to this line list by making changes to *gf* values and to the wavelengths of some lines in order to improve the fit to the solar spectrum. At this time, since we also needed our models to match the spectrum of cooler giants, we also began a comparison with the spectrum of Arcturus. We also improved our treatment of the radiative damping. Comparison of entries in Tables 4, 5, and 6 show that changes which are hard to detect at the temperature of the Sun are greatly magnified at lower temperatures, e.g., a change in the log *gf* of the Ca I 4227 line of 0.3 dex causes a change in the Ca4227 index for the 6200/4.1 model of 0.14 Å and this jumps to 1.2 and 1.0 Å for the cool giant and dwarf, respectively. This work can be considered as our initial calculations.

Comparisons of our initial calculations with the Lick indices then disagreed more than expected in some cases. While it was subsequently found that this could sometimes be due to errors in the bandpasses used, we carried out further improvements to the line list using more stringent criteria for the fits (a process similar to weeding in that it need never end). Examples of the resulting spectra are shown as Figs. 1 and 2 for the Sun and Arcturus.

We consider the fit of our synthetic indices to the observations to offer gratifying support for future work on integrated spectra. However, it is also clear that some indices are much more valuable than others in integrated spectrum work, while previously unexpected pitfalls may also exist in the response of certain indices to individual chemical species. One way of summarizing the sensitivities of the indices to the different element abundances is to ask which abundance changes cause index variations of more than twice the standard error. Few such changes are seen for the turnoff star ( $T_{\text{eff}}/\log g = 6200/4.1$ )—G4300, Fe4668, and Mg<sub>1</sub> being affected by the carbon change and Mg<sub>2</sub> and Mg *b* by the Mg change (Mg<sub>1</sub> is much less affected since it contains only very weak MgH lines but not the stronger Mg I lines). The cooler models show richer effects. Changes in the carbon abun-

dance affect CN<sub>1</sub>, CN<sub>2</sub>, Ca4227, G4300, Fe4668, Mg<sub>1</sub>, Mg<sub>2</sub> (and Mg *b* in cool giants), and the TiO indices. Changes in the oxygen abundance will also affect these indices. In addition, nitrogen abundance changes affect CN<sub>1</sub> and CN<sub>2</sub>, while changing the overall metal abundance changes CN<sub>1</sub>, CN<sub>2</sub>, Fe4668, Mg<sub>1</sub>, Mg<sub>2</sub>, Mg *b* (in cool giants), and Na D. While changes in Ca, Mg, and Na affect Ca4227, Mg<sub>1</sub>, Mg<sub>2</sub>, Mg *b*, and Na D, the Fe4383 index depends more on the Fe abundance than on [M/H].

It is obvious that the abundance of C is an important factor in many of these indices, via the strength of CN, CH, and C<sub>2</sub> lines. The abundance of oxygen will also be important in cool stars, since it controls the depletion of C via CO formation. The interpretation of many indices, particularly in integrated spectra, will also be complicated by the observed variation (Kjaergaard *et al.* 1982) of carbon abundance with evolutionary status in K giants and possible initial variations of [C/Fe]. Figure 11 suggests that the depletion of the C<sub>2</sub> lines by a change of 0.2 dex produces the same index change as a factor of 0.3 dex in overall metal abundance for the Fe4668 index.

Our conclusions on the dependence of Fe4668 on the C abundance suggest that it is risky to use this index alone in an attempt to find the abundance of galaxies, as was attempted for M32 by Jones & Worthey (1995). The variation of carbon abundance with evolutionary state and the unknown percentage of strong CN stars cause uncertainty in the value of the overall metal abundance which is deduced. It seems preferable to use either the 4383 index, with its cleaner sensitivity to abundance, or a combination of indices. It may also be necessary to supplement the Lick indices with additional data, such as observations of the CO bands.

It is also apparent from Table 3 that an increase in microturbulent velocity of 1 km/s causes a greater change in most indices than does a doubling of the overall metal abundance. The exceptions are CN<sub>1</sub>, CN<sub>2</sub>, Fe4668, Mg<sub>1</sub>, Mg<sub>2</sub>, Mg *b*, and Na D. Since microturbulence is believed to increase with decreasing gravity, these indices should be preferred for abundance determinations of stars of unknown gravity. However, we recognize that these indices primarily give abundances of specific elements, namely, C, N, Mg, and Na.

Finally, due to the large volume of data, we have chosen not to tabulate the full array of calculated spectral indices here. However, we will provide these data upon request so that any potentially useful combinations of indices (for example, [MgFe] and ⟨Fe⟩, Gonzalez 1993) may be derived from the original quantities which we have computed.

This research was supported by NSF Grants No. AST-9122361 and No. AST-9314931. Many helpful conversations with Guy Worthey are gratefully acknowledged. We thank G. Nave for sending us an electronic version of the new Fe I multiplet table, P. F. Bernath for sending electronically data from the paper by Bernath *et al.* 1991, and V. K. Bell for help in digitizing the Arcturus spectrum.

## REFERENCES

- Bell, R. A., & Gustafsson, B. 1978, *A&AS*, 34, 229  
Bell, R. A., & Gustafsson, B. 1989, *MNRAS*, 236, 653  
Bell, R. A., Paltoglou, G., & Tripicco, M. J. 1994, *MNRAS*, 268, 771  
Bell, R. A., & Tripicco, M. J. 1996 (in preparation)  
Bembenek, Z., Kepa, R., Para, A., Rytel, M., Zachwieja, M., Janjić, J. D., & Marx, E. 1990, *J. Molec. Spectrosc.*, 139, 1  
Bernath, P. F., Brazier, C. R., Olsen, T., Hailey, R., Fernando, W. T. M. L., Woods, C., & Hardwick, J. L. 1991, *J. Molec. Spectrosc.*, 147, 16  
Blackwell, D. E., & Willis, A. 1977, *MNRAS*, 180, 169  
Buzzoni, A. 1995, *ApJS*, 98, 69  
Chavez, M., Malagnini, M. L., & Morossi, C. 1995, *ApJ*, 440, 210  
Conti, P. S., & Deutsch, A. M. 1967, *ApJ*, 147, 368  
Edvardsson, B. 1988, *A&A*, 190, 148  
Idiart, T. P., & Freitas Pacheco, J. A. 1995, *AJ*, 109, 2218  
Gerö, L. 1941, *Z. Phys.*, 118, 27  
Gonzalez, J. J. 1993, Ph.D. thesis, UC Santa Cruz  
Griffin, R. F. 1968, *A Photometric Atlas of the Spectrum of Arcturus* (Cambridge Philosophical Society, Cambridge)  
Gustafsson, B., Bell, R. A., Eriksson, K., & Nordlund, A. 1975, *A&A*, 42, 407  
Gustafsson, B., & Bell, R. A. 1979, *A&A*, 74, 313  
Gustafsson, B., Kjaergaard, P., & Andersen S. 1974, *A&A*, 34, 99  
Jones, L. A., & Worthey G. 1995, *ApJ*, 446, L31  
Kjaergaard, P., Gustafsson, B., Walker, G. A. H., & Hultquist, L. 1982, *A&A*, 115, 145  
Krupp, B. M. 1973, Ph.D. thesis, University of Maryland  
Kurucz, R. L., Furenlid, I., Brault, J., & Testerman, L. 1984, *Solar Flux Atlas from 296 to 1300 nm* (National Solar Observatory, Sunspot)  
Larsson, M., & Siegbahn, P. E. M. 1983, *J. Chem. Phys.*, 79, 2270  
Larsson, M., & Siegbahn, P. E. M. 1986, *J. Chem. Phys.*, 85, 4208  
Luck, R. E., & Challener, S. L. 1995, *BAAS*, 27, 828  
McQuitty, R. G., Jaffe, T. R., Friel, E. D., & Dalle Ore, C. M. 1994, *AJ*, 107, 359  
Moore, C. E. 1945, *A Multiplet Table of Astrophysical Interest* (Revised Edition), Contributions from the Princeton University Observatory, No. 20  
Nave, G., Johansson, S., Learner, R. C. M., Thorne, A. P., & Brault, J. W. 1994, *ApJS*, 221, 687  
Tripicco, M. J. 1993, in *The Globular Cluster-Galaxy Connection*, edited by G. H. Smith and J. P. Brodie (ASP, San Francisco), p. 432  
Tripicco, M. J., & Bell, R. A. 1991, *AJ*, 102, 744  
Tripicco, M. J., Dorman, B., & Bell, R. A. 1993, *AJ*, 106, 618 (TDB93)  
Worthey, G., Faber, S. M., & González, J. J. 1992, *ApJ*, 398, 69  
Worthey, G., Faber, S. M., González, J. J., & Burstein, D. 1994, *ApJS*, 94, 687